High-temperature EPR in superionic fluorites

J. Shinar and V. Jaccarino
Department of Physics, University of California, Santa Barbara, California 93106
(Received 23 August 1982; revised manuscript received 10 January 1983)

The EPR of the Mn^{2+}-doped superionic conducting fluorites CaF_2, SrF_2, and BaF_2 has been studied at high temperatures at 9.3 GHz, and that of PbF_2 and $SrCl_2$ at 22 GHz as well. In the fluoride compounds, the ^{19}F transferred hyperfine structure (hfs) that is superimposed upon each ^{55}Mn hfs component is observed to collapse when the F^- hopping rate w^- exceeds the ^{19}F hfs coupling $A^{(19)}/\hbar$. The integrated intensity, $m^{(55)}$, and frequency dependence of the line profiles have been used to identify (in addition to static dipolar broadening) *three* distinct line-broadening mechanisms: (1) a quasistatic, nonlocal distortion of the cubic crystal field that results from the growth of ion disorder with increasing T, (2) a local, dynamic broadening related to enhanced anharmonic phonon effects, and (3) a combined *Mn^{2+}-concentration*— and T—dependent "collision" broadening which proceeds via dipolar encounters between diffusing Mn^{2+} ions and is proportional to their hopping rate, w^+. The latter mechanism is closely related to the effects of "magnetic tagging" on the ^{19}F NMR relaxation in Mn-doped PbF_2.

I. INTRODUCTION

The fluorite-structure—type superionic conductors (e.g., PbF_2) have become of increasing interest in the systematic study of anion-sublattice disorder.[1] One reason for this is that there are large differences in the anion mobility and the degree of disorder, as a function of temperature, in the isostructural compounds CaF_2, SrF_2, BaF_2, PbF_2, and $SrCl_2$. These systems have been explored with a variety of experimental and theoretical techniques.[2–4] In the present work we survey and compare the effects that rapid-ion motion have on the EPR of Mn^{2+} impurity substitutionally doped for the cations in the fluorites.

While NMR has been extensively employed to characterize the ion motion in "pure" superionic conductors, it is only relatively recently that magnetic atoms have been introduced in an attempt to "tag" the microscopic character to the motion from the effects they produce on the nuclear relaxation rates $1/T_1$ and $1/T_2$.[5,6] Complementary to the NMR work, a high-temperature study of the EPR of Mn^{2+} in PbF_2 was made in our laboratories.[7] This first use of EPR as a probe in superionic conductors gave two interesting results: (1) As the temperature increased, the ^{19}F transferred hyperfine structure (hfs) that is superimposed on each ^{55}Mn hfs component collapsed as the F^- hopping rate w^- became comparable with the hfs coupling $A^{(19)}/\hbar$; and (2) at still higher temperatures, the linewidth (ΔH) showed a dependence on the ^{55}Mn nuclear quantum number $m^{(55)}$ at high temperatures which was interpreted as resulting from dynamic crystal-field modulation.

In the present work we extend the latter study to include the concentration (c) dependence, if any, of ΔH vs T in Mn^{2+}-doped PbF_2 and CaF_2, SrF_2, BaF_2, and $SrCl_2$ as well. A related study was made of Fe^{3+} in PbF_2 and will be reported elsewhere.

Our effort was directed towards understanding the c and T dependence of the dynamical contributions to the linewidth. These can only be investigated at temperatures above which the ^{19}F transferred hfs has totally collapsed. In this high-temperature region one does not expect the linewidth to be anisotropic and, therefore, no attempt was made to study the angular dependence in single crystals.[3,8] In fact, because it is much easier to prepare random dispersions of the dopant by rapid quenching from the melt, only polycrystalline materials were used in this investigation. Doing so had the additional advantage that a maximum filling factor for the EPR sample holder could be achieved, an essential consideration in this work because the signal-to-noise ratio deteriorates rapidly at the very high temperatures for various reasons.

Spin Hamiltonian

The spin Hamiltonian describing the electronic spin energy levels of a single Mn^{2+} ion substituted for the divalent cation of fluorite-type crystals is given by[7,8]

$$\mathcal{H}=g\mu_B\vec{H}\cdot\vec{S}+A^{(55)}\vec{I}^{(55)}\cdot\vec{S}+\sum_{i=1}^{8}\vec{S}\cdot\overleftrightarrow{A}_i^{(19)}\cdot\vec{I}_i^{(19)} . \quad (1)$$

The first term is the Zeeman splitting, the second the hfs interaction between the electronic and nuclear spins of $^{55}Mn^{2+}$, and the third the transferred hfs of the Mn^{2+} spin with the eight, $I=\frac{1}{2}$, ^{19}F nuclei of the sc anion cage surrounding it. Not included is a cubic-field splitting term [shown to be negligibly small in Mn:CaF_2 (Ref. 8) and in Mn:PbF_2 (Ref. 7)] or the ^{55}Mn or ^{19}F nuclear Zeeman terms. Although inclusion of the latter was necessary to reproduce the single-crystal spectra of Mn:CaF_2 in detail,[8] it is unimportant in understanding the powder EPR of Mn in fluorites. In the case of $SrCl_2$ the last term in (1) would be replaced by a Mn^{2+}-$^{35,37}Cl$ transferred hfs interaction, which is considerably smaller.

First, consider the effects of the ^{55}Mn hfs on the EPR spectrum, above. At a constant frequency ω_0, the allowed electronic transitions ($m \equiv m^{(55)}$) $|M-1,m\rangle \rightarrow |M,m,\rangle$, to third order in $A^{(55)}/H$, occur at fields H given by[8]

$$H = H_0 - A^{(55)}m - [(A^{(55)})^2/2H][I(I+1)-m^2-m(2M-1)] - [(A^{(55)})^3/2H^2]\{(2M-1)[2I(I+1)-3m^2]-m[S(S+1)+I(I+1)-2-m^2]+3mM(M-1)\}, \quad (2)$$

where $H_0=\hbar\omega_0/g\mu_B$. Note that the second-order term induces a fine-structure splitting of the otherwise degenerate electronic transitions resulting in a nearly symmetric (*vis-á-vis* $m \leftrightarrow -m$) m dependence to the absorption line shape. The contribution of the third-order term is to destroy this symmetry, causing the different electronic transitions of the $m=+\frac{1}{2}$ hfs (higher field; $A^{(55)}<0$) component to almost collapse into a single line.[9] Model Mn^{2+} EPR spectra derived from only the Zeeman and $A^{(55)}$ hyperfine terms (up to third order) are shown in Fig. 1, and the values of H corresponding to some of the transitions are shown in Table I. To produce the synthetic spectra we have chosen $H_0=3319$ G (corresponding to an X-band frequency of 9.29 GHz) in Fig. 1(a), and $H_0=7920$ G (corresponding to a K-band frequency of 22.2 GHz) in Fig. 1(b). $A^{(55)}=-95$ e·G (see Sec. III for the experimental results of $A^{(55)}$ in these fluorites) and a derivative peak-to-peak linewidth $\Delta H_{pp}=8$ G, which is comparable to the residual widths observed in our measurements (cf. Sec. III), as discussed in Sec. IV.

Although the different electronic (fine-structure) transitions are not resolved when $\Delta H_{pp} \gtrsim 8$ G, they do produce the particular m dependence of the linewidths and lineshapes shown in Fig. 1. If, for some reason, only the $M_s=\frac{1}{2} \leftrightarrow M_s=-\frac{1}{2}$ transition was observable, then the $m^{(55)}$ dependence of the line shape would be quite different. This characteristic $m^{(55)}$ dependence then becomes a signature of the presence of all of the electronic transitions in an experimental observation, a point which is crucial to the identification of the broadening mechanisms in the superionic regime. It is interesting to note that the model spectrum shown in Fig. 1(a) closely resembles that of Mn^{2+} in aqueous solutions[10,11] without recourse to consideration of dynamic modulation of the crystal field.

Inclusion of the ^{19}F transferred hfs in Eq. (1) results in a further splitting of the electronic transitions. In CaF_2, SrF_2, BaF_2, and PbF_2 with $\vec{H}_0||[100]$, $A^{(19)} \equiv (\frac{1}{3}A_{||}^2+\frac{2}{3}A_{\perp}^2)^{1/2}$ is of the order of 10 e G.[7,8,12] If the "intrinsic" width of the electronic transition is small (approximately less than 2 G),

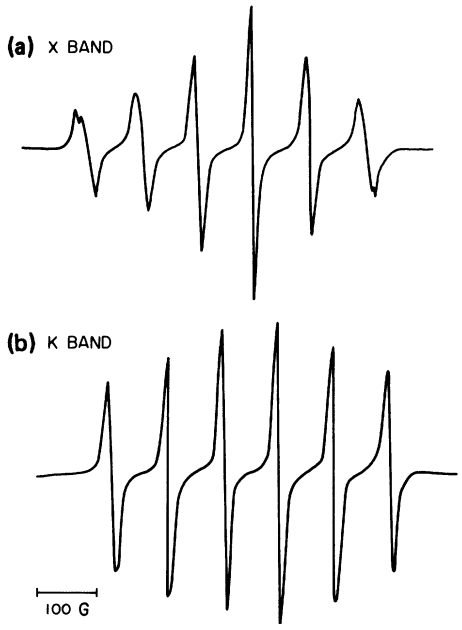

FIG. 1. Model EPR spectrum of Mn^{2+} including Zeeman and ^{55}Mn hfs term up to third order in $A^{(55)}/H$ (see text), $A^{(55)}=-95$ e G. (a) X-band spectrum, $H_0=3319$ G. (b) K band, $H_0=7920$ G. The peak-to-peak linewidth of each electronic $|M-1,m^{(55)}\rangle \rightarrow |M,m^{(55)}\rangle$ transition is $\Delta H_{pp} \equiv 8$ G. Note that the distinct $m^{(55)}$ dependence of the width and amplitude of each of the six hyperfine components is considerably larger at X band than at K band.

TABLE I. The fields for resonance of particular $|M,m^{(55)}\rangle \leftrightarrow |M-1,m^{(55)}\rangle$ transitions at (a) X band ($\nu_0=9.29$ GHz, $H_0=3319$ G) and (b) K band ($\nu_0=22.2$ GHz, $H_0=7920$ G). Here $A^{(55)}=-95\,e$ G.

$M-1\leftrightarrow M$	$-\frac{5}{2}$	(55) $+\frac{1}{2}$	$-\frac{5}{2}$
		(a)	
$-\frac{5}{2}\leftrightarrow-\frac{3}{2}$	3063.2	3355.2	3566.4
$-\frac{3}{2}\leftrightarrow-\frac{1}{2}$	3071.4	3354.9	3559.2
$-\frac{1}{2}\leftrightarrow\frac{1}{2}$	3079.0	3354.8	3552.5
$\frac{1}{2}\leftrightarrow\frac{3}{2}$	3085.8	3354.8	3546.3
$\frac{3}{2}\leftrightarrow\frac{5}{2}$	3092.0	3354.9	3540.6
		(b)	
$-\frac{5}{2}\leftrightarrow-\frac{3}{2}$	7675.2	7963.4	8161.7
$-\frac{3}{2}\leftrightarrow-\frac{1}{2}$	7678.2	7963.0	8158.8
$-\frac{1}{2}\leftrightarrow\frac{1}{2}$	7681.2	7962.6	8156.0
$\frac{1}{2}\leftrightarrow\frac{3}{2}$	7684.2	7962.3	8153.2
$\frac{3}{2}\leftrightarrow\frac{5}{2}$	7686.2	7962.0	8150.6

as is the case for CaF_2 and SrF_2 at room temperature,[8,12] the resulting spectrum will be quite anisotropic and complex, except for the $m=+\frac{1}{2}$ component when $\vec{H}_0||[100]$.[8] If the "intrinsic" width is about 5 G or larger, as it is in PbF_2 at 77 K,[7] and BaF_2 at 300 K,[12] then a partially resolved ^{19}F hfs is superimposed on each of the ^{55}Mn hfs components.

Since the ^{19}F hfs is highly anisotropic, it will produce a complex structure in a powder spectra at low Mn concentrations (approximately less than 0.05 at.%) and become unresolved at higher concentrations. In the unresolved spectra each ^{55}Mn hfs component then will appear to have a breadth which is the envelope of the unresolved ^{19}F hfs [cf. Sec. III) and Fig. 2(a)].

The above description of the EPR spectrum of Mn^{2+} is only valid in the "rigid" limit, i.e., when the contributions of anharmonic processes to the linewidths are negligible and the F^- hopping rate is small compared to the frequency separation of the individual ^{19}F hfs components $\Delta\omega^{(19)}\simeq A^{(19)}/\hbar$. As w^- approaches $\Delta\omega^{(19)}$, the individual ^{19}F hfs components will begin to broaden and merge into a single structureless line.[7,13,14] As w^- exceeds $\Delta\omega^{(19)}$, this single line narrows in proportion to $\Delta\omega^{(19)}/w^-$ until, at some higher temperature, it reaches a residual width determined by other relaxation processes.

The temperature-dependent interplay between the motional narrowing of the ^{19}F hfs and the dynamic processes contributing to the line broadening complicates what is being observed experimentally in a measurement of the peak-to-peak derivative width of a given ^{55}Mn hfs component. To simplify the notation we use only a single quantity ΔH_{pp} to designate *all* derivative peak-to-peak separations, whatever their origins. When a distinction is to be made as to the cause of the line broadening in different temperature regions, for a particular compound, it will be clearly stated in the text and figure captions.

II. EXPERIMENTAL PROCEDURE

All samples were prepared by N. Nighman in the Materials Preparation Laboratory of the Physics Department of the University of California, Santa Barbara. The preparation of PbF_2 samples required the use of Merck suprapure PbF_2 as starting material, which was first baked at 200 °C (in a vacuum of 10^{-4} Torr for 2–3 d). After backfilling with 99.996% pure N_2 gas it was transferred to the crystal growing furnace where it was then heated in an HF atmosphere above its melting point and rapidly cooled. The resulting polycrystalline material (hereafter referred to as "freshly ground") was used as starting material for all samples. Polycrystalline samples were prepared by mixing the appropriate amount of MnF_2 with the freshly ground PbF_2 or other fluoride. The mixture was heated in HF to above the melting point for about 1–2 h, and the furnace was then shut off. No effort was made to obtain single crystals, since (a) our primary concern was with disordered state properties, (b) powder samples provide a better filling factor in the BN crucible that was inserted in the microwave cavity (see below) than would a single crystal and hence yield a better signal-to-noise ratio, and (c) deleterious effects of sample conductivity at high temperatures on the Q of the cavity (through the skin effect) were considerably smaller for powder samples than for single crystals. The irreversibility of the orthorhombic- (α) to cubic- (β) phase transition in Mn:PbF_2 with T has already been established in previous studies.[6,7] Our results here are appropriate to the β phase.

Samples of Mn:$SrCl_2$ were prepared by initially drying commercial Alpha ultrapure $SrCl_2$ powder at several hundred degrees for several hours, and then mixing it, in an inert atmosphere, with the appropriate amount of $MnCl_2$. The powder mixture was heated to above the melting point of $SrCl_2$ (875 °C) in an inert atmosphere for 1–2 h and then cooled. Finally, a part of the resulting boule was crushed in a dry atmosphere and sealed in a quartz tube. We note, however, that $SrCl_2$ is notoriously hygroscopic.[15,16] Our samples may not be as ideal as those single-crystal specimens prepared for conductivity measurements by Beniere *et al.*[15]

A detailed description of the X-band EPR system used in experiments has been given.[17,18] The oven

consists either of alumina (for measurements on PbF_2) or quartz (for measurements on other fluorites) tubes coated with platinum strips that serve as heating elements. Unfortunately, either Coors or Omega alumina tubes contain trace amounts of Fe_2O_3 which produce a small background signal at $g=2$. Although this background signal could be subtracted from the EPR spectrum of Mn^{2+} in PbF_2, it introduces some uncertainty in the determination of the high-temperature linewidths.

The K-band spectrometer was similar to the X band one except that its cavity was cylindrical and sustained the TE_{011} mode. Because of its sensitivity, only thin-walled quartz tubes with very narrow Pt strips could be used with this cavity. Even so, sample conductivity losses were more severe at K band than at X band. Consequently, the K-band measurements were limited to temperatures below about 700 K.

Polycrystalline or powdered samples were placed in specially machined, pyrolytic BN crucibles. Inside the oven the crucible was supported by a Pt—Pt—13 at. % Rh thermocouple. For measurements on PbF_2 it was necessary to maintain a flow of HF-He or HF-N_2 mixture to avoid oxidation above 200 °C. Details of this flow system are given elsewhere.[18] For measurements on the other fluorites, an inert gas flow was sufficient. Note that the concentration c of Mn^{2+} in at. % represents the ratio

$$c_{Mn}/(c_{Mn}+c_{Pb})\simeq c_{Mn}/c_{Pb}\ .$$

III. EXPERIMENTAL RESULTS

A. ^{19}F and ^{55}Mn hyperfine structure

Representative powder spectra of 0.5 and 0.15 at. % (nominally 0.25 at. %) at various temperatures are shown in Fig. 2. The lineshape of each ^{55}Mn hfs component, at low temperatures, is the envelope of all of the ^{19}F transferred hfs averaged over all orientations of the field relative to the axes of the ^{19}F hfs tensor (see Sec. I). This envelope is expected to collapse when the ^{19}F hopping rate w^- approaches the transferred hfs frequency $A^{(19)}/\hbar\simeq(1.5\pm0.3)\times10^8$ sec^{-1} in CaF_2, SrF_2, BaF_2,[12] and PbF_2.[7] Indeed, this collapse is observed above 1000 K in CaF_2 (Fig. 3) and SrF_2 (Fig. 4), 800 K in BaF_2 (Fig. 5), and 400 K in PbF_2 (Figs. 6 and 7).

The X-band PbF_2 results are in agreement with those previously reported.[7] It is only beyond this envelope collapse that the actual width of the absorption line is directly observable, "unmasked" by the ^{19}F transferred hfs. In all of the fluorides, immediately following the collapse of the ^{19}F hfs, the EPR spectrum resembles that shown in Fig. 2(b). In SrF_2

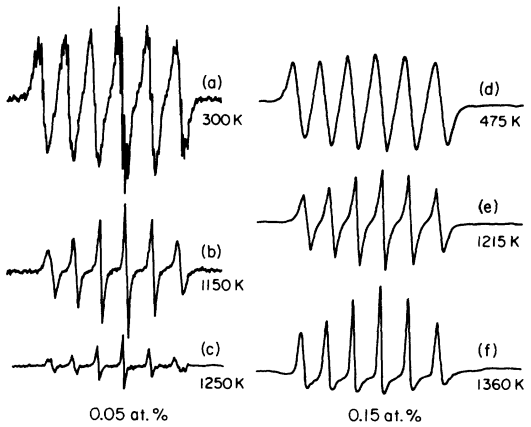

FIG. 2. Powder spectra of 0.05 and 0.15 at. % (nominally 0.25 at. %) Mn:CaF_2 at various temperatures. Note the broadening caused by the ^{19}F transferred hfs in (a) and (d), the narrow and strongly $m^{(55)}$-dependent lines in (b) and (e) and the Dysonian shapes in (f), caused by the conductivity of large crystallites in the 0.15 at. % sample (see Sec. II). All Mn concentrations are in atomic percent.

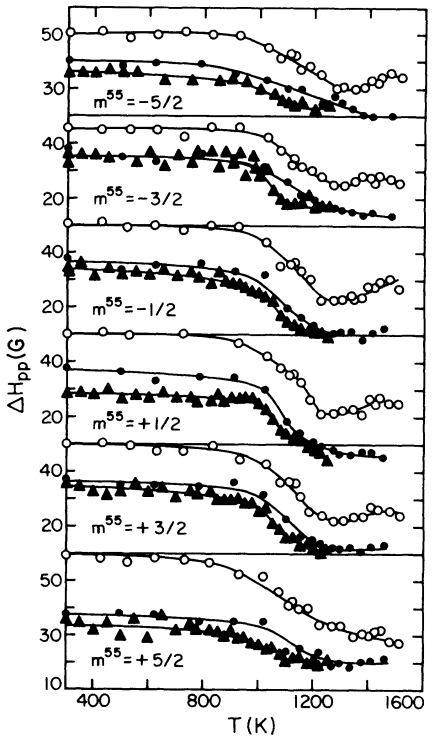

FIG. 3. Temperature dependence of the peak-to-peak width ΔH_{pp} of each ^{55}Mn hfs component in Mn^{2+} concentrations c of 0.05 at. % (▲), 0.15 at. % (nominal 0.25 at. %) (●), and 0.7 at. % (nominal 1 at. %) (○) Mn:CaF_2. Note the collapse of the ^{19}F transferred hfs from 1000 to 1200 K and the dependence of the rate of broadening at the highest T and c. See Fig. 2 caption.

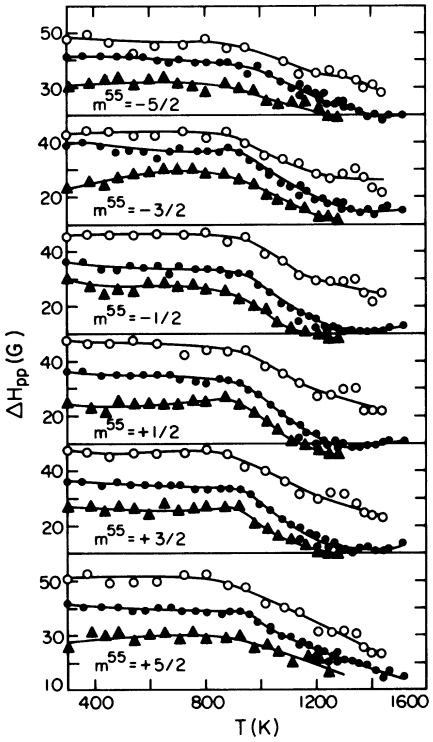

FIG. 4. Temperature dependence of ΔH_{pp} of each ^{55}Mn hfs component in concentrations of 0.05 at. % (▲), 0.22 at. % (nominal 0.25 at. %) (○), and 0.68 at. % (nominal 1 at. %) (●) Mn:SrF_2. Note the absence of any broadening at high T. See Fig. 2 caption.

and BaF_2 the $m^{(55)}$ dependence of the linewidths is as striking as it is in CaF_2 [Fig. 2(b)], but in PbF_2 it is noticeably less so (see also Ref. 7).

In Mn:$SrCl_2$ (Fig. 8), the envelope width originating from the ^{35,37}Cl transferred hfs is very small even at room temperature, and the asymmetric $m^{(55)}$

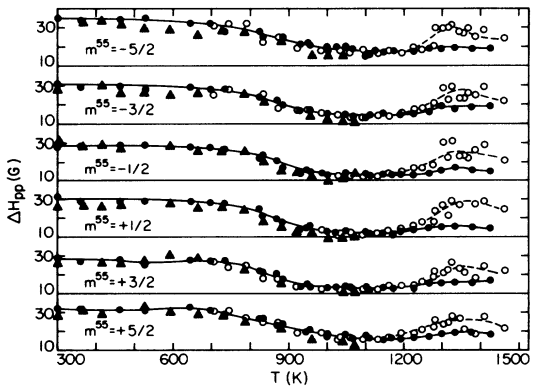

FIG. 5. Linewidth of each ^{55}Mn hfs component in nominally 0.25 at. % (●) at 1.0 at. % (○) Mn:BaF_2. Note the concentration-dependent broadening at the highest temperatures. See Fig. 2 caption.

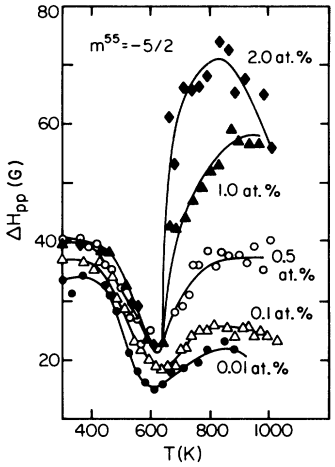

FIG. 6. $m^{(55)}=-\frac{5}{2}$ ^{55}Mn hfs component envelope widths for various Mn concentrations in Mn:PbF_2. Note the dramatic concentration dependence to the rate of broadening above 625 K. See Fig. 2 caption.

dependence at X band is as marked as it is in Fig. 2(b). Note the strong similarity to the X-band and K-band spectra shown in Fig. 1. The resemblance at X band extends to the asymmetry of the absorption

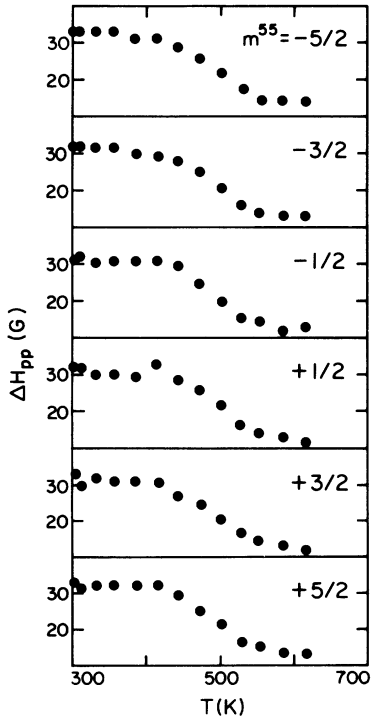

FIG. 7. Envelope widths of the various ^{55}Mn hfs components for 0.01 at. % Mn:PbF_2 at K band. Note that the $m^{(55)}$ dependence of the envelope widths is smaller here than at X band at all temperatures. See Fig. 2 caption.

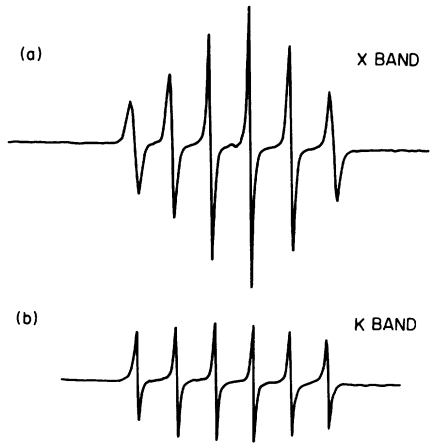

FIG. 8. Powder spectra of 0.1 at. % $Mn:SrCl_2$ at room temperature. (a) X band, $\nu_0=9.29$ GHz; (b) K band, $\nu_0=22.2$ GHz. Note the resemblance to the synthetic spectra in Fig. 1. See Fig. 2 caption.

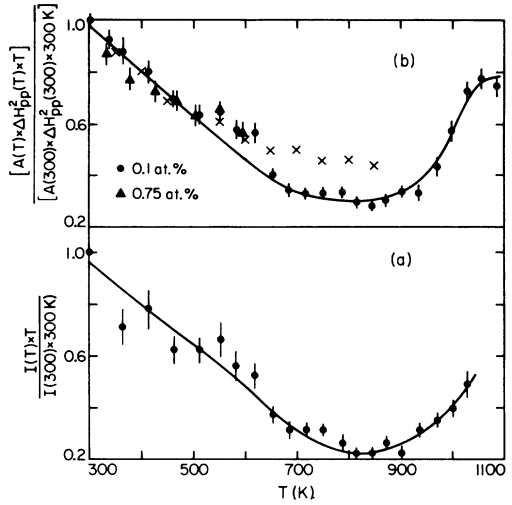

FIG. 9. (a) Integrated intensity (taking the Boltzmann factor into account) of 0.1 at. % $Mn:SrCl_2$ as a function of temperature. (b) The product (amplitude)$\times$(envelope width)$^2\times$(Boltzmann factor), summed over the six ^{55}Mn hyperfine components, of 0.1 at. % $Mn:SrCl_2$. The crosses are the predictions of the model discussed in Sec. IV B. See Fig. 2 caption.

derivative of the outer components ($m^{(55)}=\pm\frac{5}{2}$) about zero, that is to say, the positive amplitude of the $m^{(55)}=-\frac{5}{2}$ ($+\frac{5}{2}$) component is slightly smaller (larger) than the negative amplitude. In Sec. I we noted that such a spectrum indicates *all* of the electronic spin transitions are being observed. However, as is shortly to be seen, intensity and linewidth measurements indicate the $Mn:SrCl_2$ "outer"-electronic transitions (i.e., $\pm\frac{5}{2}\leftrightarrow\pm\frac{3}{2}$ and $\pm\frac{3}{2}\leftrightarrow\pm\frac{1}{2}$) broaden significantly above 300 K.

B. Intensity measurements

Since the fine structure is not resolved in our spectra, only relative intensity measurements can determine how severely the different electronic transitions broaden as a function of temperature. The integrated intensity, which is proportional to the Q of the cavity divided by the absolute temperature, was determined by integrating the absorption derivative spectra twice using a Nicolet model 1072 Instrument Computer. Because only at elevated temperatures did the high conductivity of these materials affect the Q, and also limit the penetration of the rf field, we restricted our measurements to temperatures below 1300 K in CaF_2 and SrF_2, 700 K in PbF_2, and 1050 K in $SrCl_2$. After taking the Boltzmann factor into account, no detectable change, beyond the $\pm 15\%$ scatter in the results, was found in the corrected integrated intensity of the XF_2 spectra. On the other hand, the corresponding $Mn:SrCl_2$ intensity is very striking in its T dependence [Fig. 9(a)]. It drops to about 25% of the room-temperature value by 850 K and then begins to increase with T until it regains its initial value at 1050 K. The X- and K-band results are quite similar in the range $T\leq 600$ K. In Fig. 9(b) the variation of the intensity versus T as reflected in the product (derivative peak-to-peak amplitude)$\times$(linewidth)^2 $\times$(Boltzmann factor) at X band is shown. (This is appropriate for $Mn:SrCl_2$ since its line shape resembles a Lorentzian at all temperatures.) This procedure yields results that are similar to those obtained from the directly integrated intensity. Both are consistent with a behavior wherein only the *non*-($\frac{1}{2}\leftrightarrow-\frac{1}{2}$) electronic transitions monotonically broaden from 300 to 800 K (the minimum intensity being reduced ideally to $\frac{9}{35}$ of its original value[19]) and then narrow once more at higher temperatures. In Sec. IV we show that to be possible if the Cl^- hopping motion induces a quasistatic disorder in the crystal.

C. Linewidth measurements

1. General observations

The X-band linewidths of each of the ^{55}Mn hfs components has been studied, as a function of Mn^{2+} concentration and temperature, for all of the XF_2 and $SrCl_2$ samples. What are actually measured are the *derivative peak-to-peak widths* ΔH_{pp}. Provided $\Delta H_{pp}\lesssim 30$ G, one may assume the overlap between adjacent ^{55}Mn hfs component line profiles, whose separation is of order 100 G, to be small, and a

"true" linewidth or envelope width may be derived from ΔH_{pp}. If the above condition is not satisfied, then the apparent widths are actually smaller than "true" widths. This problem is most clearly seen by integrating the absorption derivative and is displayed in Fig. 10. Thus it is difficult to determine the intrinsic broadening in the presence of the ^{19}F hfs in the XF_2 compounds. At the higher temperatures, where the ^{19}F hfs has collapsed, it is possible to isolate the separate contributions to the broadening, including the $m^{(55)}$-dependent fine-structure splitting. In the superionic region the line shapes become Dysonian but, because the ^{55}Mn hfs overlap effects are usually small, the "true" widths may be determined using the now standard method described by Peter *et al.*[20]

Since the transition $(M,m^{(55)}=+\frac{1}{2}\leftrightarrow M\pm 1, m^{(55)}=+\frac{1}{2})$ exhibits no fine structure, its width was used to identify those contributions to the broadening that were concentration (c) dependent, temperature (T) dependent, or both, but *not* $m^{(55)}$ dependent. Thus it was possible to establish that there is (1) a c-dependent, but T-independent, broadening, (2) a c-dependent *and* T-dependent broadening, and (3) a c-independent, but T-dependent, contribution to the linewidths. The first originates with the Mn^{2+} dipole-dipole interaction, the second with "collision" broadening caused by Mn^{2+} diffusion, and the third may be regarded as having two sources: (a) a quasistatic broadening related to the modulation of the crystal field, and (b) a dynamic anharmonic phonon-induced broadening. We now consider the evidence for each of these in turn.

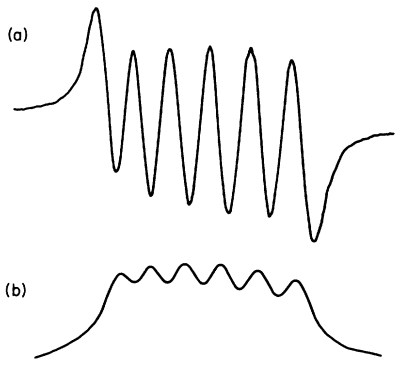

FIG. 10. (a) Absorption derivative of 0.7 at. % (nominally 1.0 at. %) Mn:CaF_2 at 300 K. (b) Absorption line shape resulting from integration of (a). Note that the overlap of the various ^{55}Mn hfs components results in apparent derivative peak-to-peak widths that are smaller than the true widths. See Fig. 2 caption.

2. *Concentration-dependent, temperature-independent broadening*

In the Mn-doped CaF_2, SrF_2, and PbF_2, a constant difference is observed between the envelope widths for different concentrations up to a temperature region where the ^{19}F transferred hfs collapses (see Figs. 3, 4, and 6). Because the envelope widths in this low-T region represent a convolution of the ^{19}F hfs and the Mn^{2+} dipolar broadening, it is difficult to extract the latter from the measured width—particularly so as the overlap between adjacent ^{55}Mn hfs line profiles distorts the individual lines, making ΔH_{pp} not representative of the "true" widths, as discussed above.

However, at the temperature at which the envelope width is a minimum, the Mn^{2+} dipolar width can be no *more* than that which is observed. Hence an *upper* bound may be placed on the dipolar contribution to the width. This is important because, as we shall see, a naive calculation of the dipolar widths gives a result in excess of the observed upper bound. In any case, we have determined that the dipolar widths ΔH_{pp} are approximately less than 30, 31, 22, and 11 G/(at. % Mn^{2+} dopant) in CaF_2, SrF_2, PbF_2, and $SrCl_2$, respectively. In Mn:BaF_2 a slow T, concentration-dependent broadening is not observed because of the small solubility[12] of Mn in BaF_2 below 900 K. In fact, the EPR of all samples with $c \geq 0.25\%$ display a broad structureless resonance, centered at G=2.0 (in addition to the six-line ^{55}Mn hfs pattern associated with the isolated impurity) whose intensity diminishes rapidly above 900 K. Because of this feature of the Mn:BaF_2 EPR, no attempt was made to determine the dipolar contribution to the broadening.

3. *Concentration-dependent, temperature-dependent broadening*

After the ^{19}F transferred hfs has essentially collapsed, a most unusual linewidth behavior is observed in Mn:PbF_2; namely, one that is *both* c and T dependent. This is apparent in Fig. 6 where the linewidth is seen to increase with increasing c and T above 600 K, reaching some broad maximum in the vicinity of 850–900 K. A careful examination of the different $m^{(55)}$ hfs components indicates this c- and T-dependent broadening is independent of $m^{(55)}$. The c dependence of the linewidth at various T in this high-temperature region is shown in Fig. 11. From the linearity of the ΔH_{pp} vs c plots, at fixed values of T, we may directly infer that this new broadening mechanism is linear in c while being strongly T dependent. We shall argue that the "collision" between diffusing Mn^{2+} ions is responsible for the c- and T-dependent broadening, in analogy

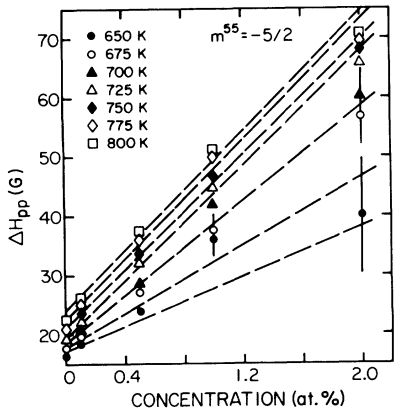

FIG. 11. Concentration dependence of the widths of the $m^{(55)}=-\frac{5}{2}$ hfs component of Mn:PbF_2 at various T. Note that the "best-fit" lines do not converge to a single point at $c=0$, indicating that a T-dependent but c-independent contribution to ΔH exists. See Fig. 2 caption.

with the "magnetic tagging" effects seen in the ^{19}F NMR in Mn:PbF_2. The latter arise from F^--Mn^{2+} encounters caused by the F^- diffusion.[5]

It is to be noted that the best-fit lines through the data in Fig. 11 do not converge to a single value at $c=0$, suggesting there is a *c-in*dependent, but T-dependent, contribution to ΔH_{pp}. This is immediately apparent from the result on the 0.01 at.% Mn:PbF_2 sample (see Fig. 6 and Ref. 7), but the intercept of the lines, at $c=0$ with the ordinate, is a more accurate determination of this quantity. We discuss the source of this mechanism next in connection with the results in Mn:$SrCl_2$.

4. Concentration-independent, temperature-dependent broadening

To a degree, a c-independent, but T-dependent, broadening may exist in all of the samples, but only in the Mn:$SrCl_2$ is it possible to isolate it clearly from other contributions to the linewidth at all temperatures. The fact that the anion transferred hfs is so much smaller for the chlorides ($\lesssim 3$ G) than the fluorides is of major help in this regard. Of somewhat equal importance is that the larger lattice constant of $SrCl_2$, relative to the XF_2, appreciably reduces the dipolar contribution to the broadening (see Sec. IV B 2). Thus it is not surprising to find no concentration dependence to the broadening in Mn:$SrCl_2$ at all temperatures, for $c \lesssim 0.5\%$, which appears to be the solubility limit.

Because the envelope widths are strongly $m^{(55)}$ dependent at low T, it is necessary to consider the T dependence of each ^{55}Mn hfs component. The $m^{(55)}$ dependence is largely, but not entirely, caused by the electronic fine-structure splitting. In Fig. 12 the outer components $m^{(55)}=\pm\frac{5}{2}$ are seen to decrease in width with increasing T below 500 K, while the $m^{(55)}=\pm\frac{1}{2}$ components (for which there is little or no fine-structure splitting) show a monotonic increase to its widths with increasing T in this same temperature region. The $m^{(55)}=\pm\frac{3}{2}$ behavior is intermediate to the other pairs. Above 600 K, all ^{55}Mn hfs components broaden monotonically with increasing T and show a very rapid increase above 900 K (see also Fig. 13).

In addition to the measurements of the line broadening we have measured the peak-to-peak amplitudes $A(m^{(55)})$ for each ^{55}Mn hfs components. The amplitude ratio

$$R=\frac{A(m^{(55)})}{A(m^{(55)}=\pm\frac{1}{2})}$$

versus T is shown in Fig. 14 and is seen to asymptotically approach unity at the highest temperatures. Now at low T, $R<1$ because of the fine-structure splitting on all but the $m^{(55)}=+\frac{1}{2}$ component. The fact that R approaches unity, for all $m^{(55)}$ at about

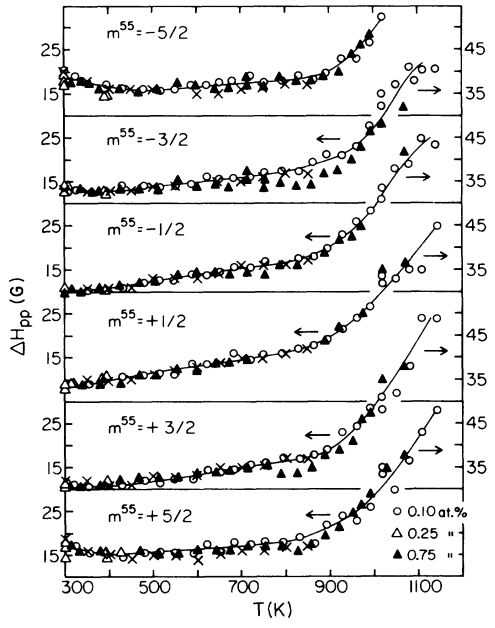

FIG. 12. Temperature dependence of the peak-to-peak widths of the six hyperfine components of the X-band EPR of Mn:$SrCl_2$. Note that while the $m^{(55)}=\pm\frac{1}{2}$ components broadens immediately above 300 K, the $m^{(55)}=\pm\frac{5}{2}$ components initially narrow before proceeding to broaden at higher temperatures. The crosses are the predictions of a model described in Sec. IV B 1. See Fig. 2 caption.

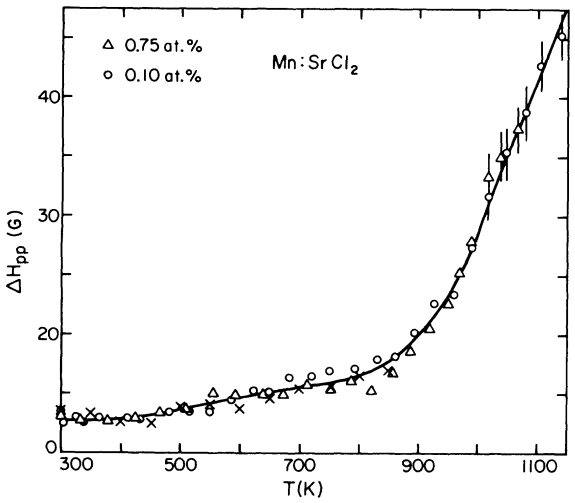

FIG. 13. Peak-to-peak widths of the Mn EPR in $SrCl_2$, averaged over the six ^{55}Mn hfs components. Note the lack of any Mn^{2+} c dependence; the widths being identical for the 0.1 at.% (○) and the 0.75 at.% (△) samples. The crosses are the predictions of a model described in Sec. IV B 1; the solid line is a guide to the eye. See Fig. 2 caption.

900 K, indicates that only the electronic $|M_s=1/2\rangle \leftrightarrow |M_s=-\frac{1}{2}\rangle$ transition is observed at these higher temperatures—a result in keeping with our conclusions from the integrated intensity studies

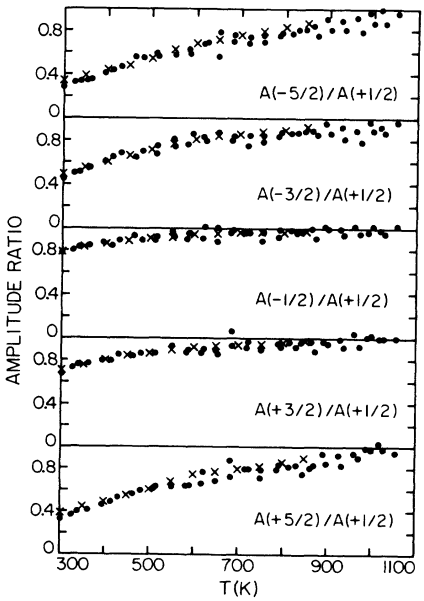

FIG. 14. Temperature dependence of the ratios of the amplitudes of the various ^{55}Mn hfs components in the EPR of 0.1 at.% Mn:$SrCl_2$ to that of the $m^{(55)}=+\frac{1}{2}$ component. The crosses are the predictions of the model described in Sec. IV B 1. See Fig. 2 caption.

(see preceding section) and that there is no discernible $M^{(55)}$ dependence on ΔH_{pp} above 900 K.

Since the Cl^- hopping rate is so small [$w^- \lesssim 2\times 10^6$ sec^{-1} at $T\simeq 660$ K in extrinsically conducting $SrCl_2$ (Refs. 15 and 16)], we cannot attribute the initial monotonic increase in $\Delta H_{pp}(+1/2)$ to a local dynamic modulation of the Mn^{2+} crystal field. Rather, we associate the broadening with a quasistatic, random, nonlocal distortion of the Mn^{2+} crystal field which serves to slowly broaden, first the outer ($M_s=\pm\frac{5}{2}\leftrightarrow M_s=\pm\frac{3}{2}$) transitions and then the inner ($M_s=\pm\frac{3}{2}\leftrightarrow M_s=\pm\frac{1}{2}$) transitions, both of which are sensitive, in first order, to axial distortions. This broadening is accompanied by the slow disappearance of intensity associated with these transitions. At higher temperatures, $T\gtrsim 900$ K, the rapid increase of ΔH_{pp} is accompanied by the restoration of intensity, indicating all electronic transitions are once again observable. We believe the broadening to arise primarily from anharmonic phonon effects, with the contribution from dynamic–crystal-field modulation being very much smaller. An attempt to understand all of the c-independent, T-dependent broadening is given in the next section.

IV. INTERPRETATION

A. Collapse of ^{19}F hfs with increasing temperature

Each of the XF_2 compounds exhibits a ^{19}F transferred-hfs interaction $\vec{I}\cdot\overleftrightarrow{A}^{(19)}\cdot\vec{S}$ with the Mn^{2+} impurity that is generally unresolved (or only partially so, at low concentrations) in a powder because of the anisotropy in the hfs. Since $|A^{(19)}| \ll |A^{(55)}|$, the ^{19}F hfs appears as a broadening of each of the ^{55}Mn hfs components. As the temperature increases so does the F^- hopping rate w^-. When w^- approaches the magnitude of $\overleftrightarrow{A}^{(19)}$, one would expect the ^{19}F hfs to begin to broaden and collapse. In the fast-hopping limit, $w^- \gg A^{(19)}/\hbar$, a single line should appear, centered at each of the ^{55}Mn hfs component resonance positions, with a width proportional to $|A^{(19)}/\hbar|^2/w^-$.[14]

Hence the observed collapse of the ^{19}F hfs as a function of increasing temperature, which is seen in Figs. 3–6, should exhibit a "universal" behavior if plotted as a function of the reduced variable $w^-/(A^{(19)}/\hbar)$. This is shown in Fig. 15 where the peak-to-peak envelope width of the $m^{(55)}=+\frac{1}{2}$ hfs component, normalized to its 300-K value, is plotted as a function of the logarithm of $w^-/(A^{(19)}/\hbar)$ for Mn^{2+} in CaF_2, SrF_2, and PbF_2 (the Mn:BaF_2 results are not displayed because of solubility problems; see Sec. III B 2). The values of w^- were obtained from

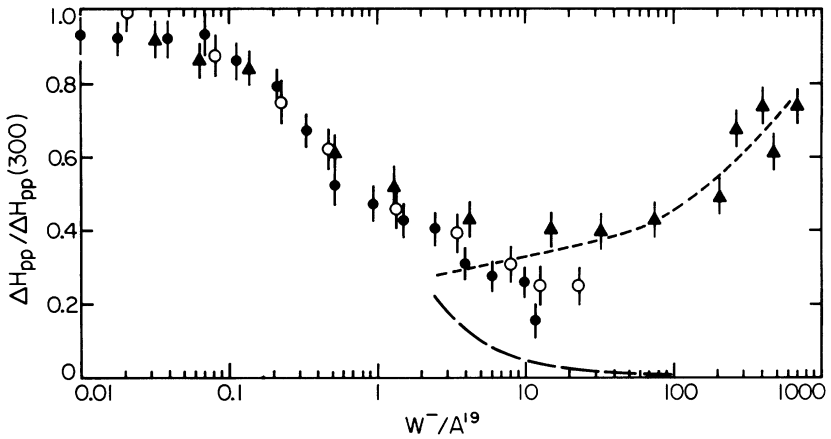

FIG. 15. Normalized envelope width of the "central" $m^{(55)}=+\frac{1}{2}$ hfs component, $\Delta H_{pp}(T)/\Delta H_{pp}(300)$, as a function of the "reduced" anion-hopping rate $\hbar w^-/A^{(19)}$ in 0.05 at.% Mn:CaF_2 (○), 0.05 at.% Mn:SrF_2 (●), and 0.01 at.% Mn:PbF_2 (△). Note the "universal" character of the collapse of the transferred hfs to what are residual widths determined by other mechanisms and the broadening of Mn:PbF_2 at high hopping rates. The theoretical residual widths are given by the long dashed lines and the difference between it and the observed width in Mn:PbF_2 is indicated by the short dashed line.

Refs. 21–23 and those of $A^{(19)}$ from Refs. 7 and 12. The normalized widths are seen to fall to approximately one-half their initial value at $w^-/(A^{(19)}/\hbar)\simeq 1$. The long dashed line is the asymptotic behavior expected in the fast-hopping limit. Although the CaF_2 results come closer to the predicted behavior at large $w^-/(A^{(19)}/\hbar)$ than either of the other two, it is clear that in all three cases the widths in this high-temperature region must be caused by other mechanisms. In particular, in PbF_2 we ascribe the increasing linewidth with increasing w^- (which is best fit by the short dashed line) to dynamic relaxation processes, as will be discussed below. In all three compounds the Mn^{2+} concentration was so small (see caption of Fig. 15) as to preclude either dipolar broadening or collision broadening between diffusing Mn^{2+} ions.

B. Temperature and concentration dependence of linewidths and intensities

Since the variation of the linewidths and intensities with temperature and the dependences of the linewidths upon Mn^{2+} concentration c differ from one system to the next, it is clear no *single* mechanism is responsible for that part of the observed line broadening not related to the ^{19}F hfs discussed above. In fact, we believe there are four distinct contributions: static dipolar, quasistatic crystal-field distortions, dynamic (single-ion, phonon, or crystal-field modulations), and, lastly, collision broadening between diffusing Mn^{2+} ions. The steps involved in separating the various contributions to the broadening include first, correlating the $m^{(55)}$ dependence of the linewidth and the EPR integrated intensity with the anion-hopping rate. This should be done for concentrations of Mn^{2+} small enough that neither dipolar nor collision broadening are of any significance at all temperatures. Then the c dependence of the broadening must be established and partitioned into its T-independent and T-dependent contributions. We begin with Mn:$SrCl_2$ because it, alone, exhibits a variation of both intensity and linewidth with temperature. The absence of any c dependence to its linewidth (other than the small dipolar contribution which we will subsequently identify) implies the broadening is of single-ion origin.

1. Quasistatic crystal-field and dynamic broadening—Mn:$SrCl_2$

The EPR results on Mn:$SrCl_2$ may be briefly summarized as follows: Although all of the electronic transitions are observable at 300 K, the outer ones (those other than the $|\frac{1}{2}\rangle\leftrightarrow|-\frac{1}{2}\rangle$ transition) become less intense with increasing T until, at 900 K, only the $|\frac{1}{2}\rangle\leftrightarrow|-\frac{1}{2}\rangle$ transition remains to be seen. This is initially accompanied by a slowly decreasing width of the outer components and an increasing width of the central ^{55}Mn hfs component and a decrease in the asymmetry of their relative widths. Above 900 K, the intensity times T monotonically increases towards its 300-K value with increasing T, indicating all of the transitions are being observed, while at the same time the width of each of the ^{55}Mn hfs components continue to increase.

This behavior of the widths (Figs. 12 and 13),

shape (Fig. 14), and intensity (Fig. 9) of the EPR spectra of Mn:$SrCl_2$ may be understood by assuming that the Cl^- hopping induces a general disorder in the fluorite crystal. Characterizing the disorder at any given Mn site by an instantaneous axial distortion, its contribution to the spin Hamiltonian may be represented by the term

$$\mathcal{H}_{ax}=D[S_{z'}^2-\tfrac{1}{3}S(S+1)]\ , \tag{3}$$

where z' is the instantaneous direction of the axial field distortion and D is its magnitude. Although the distortion may include an orthorhombic component, the latter's effect would be indistinguishable from an axial one in our case. The axial field induces a fine-structure splitting of the different electronic transitions which, in a strong magnetic field, is given by (to second order in D/H)[24]

$$h\nu(M\rightarrow M-1)=g\mu_B H+D(M-\tfrac{1}{2})(3\cos^2\theta-1)-\frac{D^2\sin^2 2\theta}{8g\mu_B H}[4S(S+1)-24M(M-1)-9]$$
$$+\frac{D^2\sin^4\theta}{8g\mu_B H}[2S(S+1)-6M(M-1)-3]\ . \tag{4}$$

As is appropriate to Mn^{2+}, g is assumed to be isotropic. What is immediately apparent from Eq. (4) is that the axial field affects the "outer" electronic transitions in first order in D and the central $|\tfrac{1}{2}\rangle\leftrightarrow|-\tfrac{1}{2}\rangle$ transition only in second order. Hence if the various axial distortions at the different Mn sites were equal and parallel to each other, a single-crystal spectrum would display a fine-structure splitting with a large angular dependence. However, if at any instant of time, the axial fields are randomly oriented with respect to H (as would especially be the case in a powder sample), then this splitting would have to be averaged over all orientations. For distortions that vary in time more slowly than $(\gamma\Delta H)^{-1}$, this would manifest itself as an inhomogeneous broadening of the otherwise degenerate electronic transitions. The absorption function of the different electronic transitions of $^6S_{5/2}$ ions in randomly oriented axial crystal fields has been treated.[25] In that case the absorption function $i(H)$ (for zero assumed linewidth) of the outer $M\neq\frac{1}{2}\rightarrow M-1$ transitions is given by

$$i(H)=\frac{N_0}{4\sqrt{3}(M-\frac{1}{2})D}\left[1-\frac{H-H_i}{D(M-\frac{1}{2})}\right]^{-1/2} \tag{5}$$

in the region

$$H_i-2D(M-\tfrac{1}{2})\leq H\leq H_i+D(M-\tfrac{1}{2})\ ,$$

and zero elsewhere. Here H_i is the field for resonance of the $M\rightarrow M-1$ transition when $D=0$ (as determined by both M and $m^{(55)}$) and N_0 is the total number of spins in the sample. This absorption function has a shoulder at $H=H_i-2D(M-\frac{1}{2})$ and a singularity at $H=H_i+D(-\frac{1}{2})$. The absorption function of the central $|\tfrac{1}{2}\rangle\leftrightarrow|-\tfrac{1}{2}\rangle$ transition is much narrower because there are no first-order terms in the expression for its resonance field [Eq. (4)], and is given by

$$i(H)=\frac{3N_0H_i}{64D^2}\left[1-\frac{9}{32}\frac{H_i(H-H_i)}{D^2}\right]^{-1/2}\left[5-4\left[1-\frac{9}{32}\frac{H_i(H-H_i)}{D^2}\right]^{1/2}\right]^{-1/2} \tag{6a}$$

in the region $H_i-2D^2/H_i\leq H\leq H_i$, and

$$i(H)=\frac{3N_0H_i}{64D^2}\left[1-\frac{9}{32}\frac{H_i(H-H_i)}{D^2}\right]^{-1/2}\sum_{n=1}^{2}\left[5+(-1)^n4\left[1-\frac{9}{32}\frac{H_i(H-H_i)}{D^2}\right]^{1/2}\right]^{-1/2} \tag{6b}$$

in the region $H_i<H\leq H_i+\frac{32}{9}(D^2/H_i)$. This absorption function has two singularities, at $(H-H_i)H_i/D^2=-2$ and $+\frac{32}{9}$ and a small shoulder at $H=H_i$.

The actual absorption derivative line shape $I'(H)\equiv dI(H)/dH$ for a finite, nonzero linewidth is given by the convolution of the derivative of the shape function $L'(H-H')$ and $i(H')$, i.e.,

$$I'(H)=\int L'(H-H')i(H')dH'\ . \tag{7}$$

From the foregoing discussion, it is clear that for any given value of $D\neq 0$, these absorption functions will not resemble the simple, six hyperfine-component experimental results. However, if we assume a *distribution* of axial fields D around $D=0$, with standard deviation σ, then a proper choice of σ and the linewidth ΔH_{pp} results in a close fit between the simulated and observed spectra. This is clearly seen in Fig. 16. In the underlying physical picture one would indeed expect D to depend on the distri-

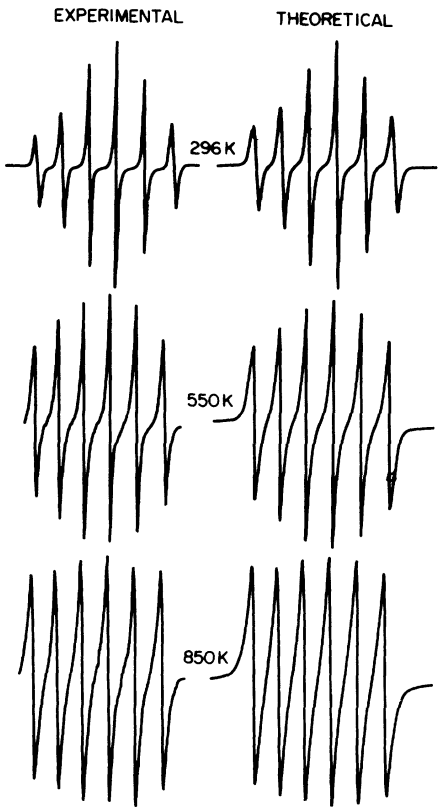

FIG. 16. Comparison between some of the synthetic spectra obtained in fitting the model described in Sec. IV B 1 and the experimental results on Mn:$SrCl_2$.

bution of vacancies around a given Mn^{2+} ion. The resultant absorption derivative line shape would therefore reflect a distribution of D values centered around $D=0$. We note that the agreement between the experimental and simulated spectra is insensitive to the type of axial field distribution. The displayed synthetic spectra were obtained from a Gaussian distribution. One might also expect σ to increase with temperature because of increased anion hopping. The "outer" electronic transitions would begin to broaden more rapidly than the $|-\frac{1}{2}\rangle \leftrightarrow |+\frac{1}{2}\rangle$ transitions with increasing T. This would be accompanied by a decrease of the $m^{(55)}$ dependence of the envelope widths and amplitudes of the six hyperfine components since both result from the $A^{(55)}$ hyperfine-interaction–induced fine-structure splitting (see Sec. I).

Specifically, this would result in an initial reduction of the envelope widths of the $m^{(55)}=\pm\frac{5}{2}$ components and an increase in the ratio of the amplitudes of these components, relative to the $m^{(55)}=+\frac{1}{2}$ component. In addition, the apparent integrated intensity [and the (amplitude)$\times$(envelope width)^2], summed over the six hyperfine components would decrease with increasing T. Indeed, all of these features are observed (Figs. 9, 12, and 14).

The temperature dependence of σ and ΔH_{pp} required to reproduce the observed spectra and its intensity are shown in Figs. 17 and 18. The temperature dependence of ΔH_{pp} is also directly observable since it is essentially the envelope width of the central $m^{(55)}=+\frac{1}{2}$ hfs component. Finally, the temperature dependence of the linewidth ΔH_{pp} not related to hfs-induced fine-structure, Cl transferred-hfs, or quasistatic crystal-field broadening is shown in Fig. 19. We shall now concentrate on the interpretation of the temperature dependence of ΔH_{pp}.

First, we note that the low-temperature values of ΔH_{pp} must also contain whatever contribution there is from the ^{35}Cl, ^{37}Cl transferred hfs. If we assume these hfs constants to be roughly $|A^{(35)}| \simeq |A^{(37)}| \leq 3$ G [about (25–30)% the value of $A^{(19)}$ in the fluorides[7,12]], then at high temperatures we expect the broadening induced by the transferred hfs to narrow out in a manner similar to that shown in Fig. 4. In that case, the actual homogeneous linewidth probably increases more rapidly than the envelope width of the $m^{(55)}=+\frac{1}{2}$ hfs component and may be roughly described by the dotted line in Fig. 19.

A similar c-independent, T-dependent broadening was previously observed in Mn:PbF_2 and confirmed in this work (see Sec. III and Figs. 6 and 11). In the earlier work, the broadening was attributed to dynamic crystal-field effects and quantitatively treated using Redfield's relaxation matrix[26,27] in a manner similar to the Mn^{2+} EPR in liquids.[10,11] Specifically, it was assumed that the anion disorder causes fluctuating axial $[D(t)]$ and/or orthorhombic $[E(t)]$ distortions around the Mn site, whose time correlation functions are given by

$$\langle Y(0)Y(t)\rangle = \langle Y^2(0)\rangle e^{-wt},$$

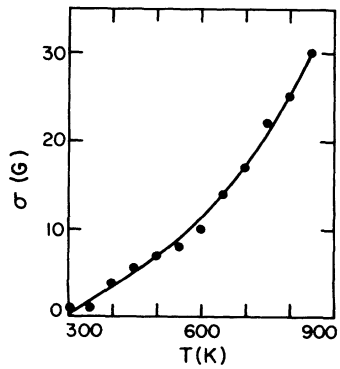

FIG. 17. Temperature dependence of σ, the standard deviation of the distribution of quasistatic axial crystal fields, used to reproduce the experimental results in Figs. 9, 12, and 14. The line is a guide to the eye.

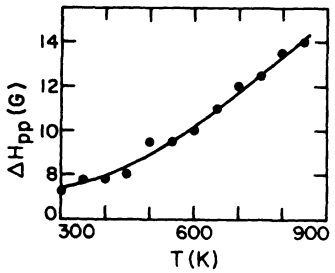

FIG 18. Residual ΔH_{pp} vs T of the $|M-1,m^{(55)}\rangle \rightarrow |M,m^{(55)}$ transitions of Mn:$SrCl_2$ used to reproduce the experimental results in Figs. 9, 12, and 14. The line is a guide to the eye.

where $Y=D$ or E and w is the anion-hopping rate. We will now show that for several reasons this mechanism cannot account for the temperature dependence of ΔH_{pp} in Mn:$SrCl_2$.

(a) A basic difference between crystal-field fluctuations in liquids and in superionic fluorites is that in the former, the amplitude of $D(t)$ or $E(t)$ is nonzero for most values of t. In the latter, $D(t)$ or $E(t)$ is nonzero only when one of the nearest neighbors (NN) of a Mn ion is a vacancy. This situation occurs roughly only a fraction c of the time, where c is the vacancy concentration. During most of the time, $D(t)$ and $E(t)$ are almost zero (except for the influence of next-NN vacancies). The resulting time correlation functions of $D(t)$ and $E(t)$ are of the form (see Appendix A)

$$\langle Y(0)Y^*(t)\rangle = \frac{c}{1+c}Y^2(0)\left[1+\frac{e^{-wt}}{1+c}e^{-w/ct}\right]. \tag{8}$$

Therefore, the "effective" amplitude of the fluctuation field is only $\sqrt{[c/(1+c)]}Y(0)$. Although $\sqrt{c/(1+c)}$ is of order unity in PbF_2, which is heavily disorderd above 700 K, in $SrCl_2$ this factor is only $\sim\frac{1}{7}$ at 1050 K (Ref. 28). (b) In addition, $\langle Y(0)Y^*(t)\rangle$ decays at the vacancy-hopping rate w/c and not the anion-hopping rate. This implies that the fluctuation rate approaches the Larmor frequency $\omega_0=6\times10^{10}$ sec^{-1} at about 650 K in PbF_2,[23,28] and approximately less than 925 K in $SrCl_2$.[15,28] However, one would then expect the linewidth to peak at those temperatures and decline at higher ones—contrary to the observed behavior of Mn:$SrCl_2$ (Figs. 12 and 13) and of 0.1 at.% Mn:PbF_2 (Fig. 6, Ref. 7). (c) Application of Redfield's theory to the problem of the fluctuating crystal fields results in an $m^{(55)}$ dependence of the linewidth opposite to the observed one (i.e., one in which the "outer" $m^{(55)}=\pm\frac{5}{2}$ hfs components are narrower than the "central" $m^{(55)}=\pm\frac{1}{2}$ ones) in the slow-hopping ($w/c \ll \omega_0$) limit.[29]

Because of the above-mentioned arguments, we are led to consider an alternative linewidth source in Mn:$SrCl_2$; namely, phonon-induced broadening. A comprehensive survey of this problem is given by Abragan and Bleaney.[30] It is there shown that at temperatures above a few degrees Kelvin, the dominant phonon-induced mechanism is the two-phonon Raman scattering. The spin-lattice relaxation rate $1/T_1$ of a multiplet ground-state Kramers doublet (such as Mn^{2+}) induced by this process is given by

$$\frac{1}{T_1}=\frac{3}{4\pi^3\rho^2v^{10}}\left[\frac{V^4}{\hbar^2}\right]\left[\frac{kT}{\hbar}\right]^5 I_4\left[\frac{T}{\Theta_D}\right], \tag{9}$$

where ρ is the crystal density (g cm^{-3}), v the sound velocity, V the matrix element between the ground state and virtual excited states, and

$$I_4\left[\frac{T}{\Theta_D}\right]=\int_0^{\Theta_D/T}[x^4e^x/(e^x-1)^2]dx, \tag{10}$$

Θ_D being the Debye temperature. This relaxation mechanism has indeed been shown[31] to be the dominant one in Mn^{2+}- and Eu^{2+}-doped XF_2 (X=Ca,Sr,Ba) at very low temperature (i.e., from 4 K to 20–30 K). However, the simple extrapolation of those results to the high-temperature limit of this model yields absurd relaxation rates for Mn:SrF_2 ($\sim4\times10^{10}$ sec^{-1} at 1000 K) and Mn:BaF_2

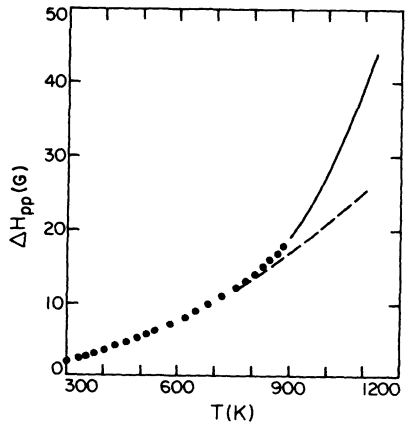

FIG. 19. Temperature dependence of the linewidth ΔH_{pp} of Mn:$SrCl_2$ without the contributions from the hfs-induced fine structure, transferred-hfs, or quasistatic crystal-field broadening is shown as a solid line. The dotted line is the estimated behavior at lower temperatures, and the dashed line is the $T^5I_4(\Theta_D/T)$ dependence discussed in Sec. IV B 1 and Eqs. (9) and (10).

($\sim 2.3\times10^{11}$ sec^{-1} at 1000 K), in total disagreement with our linewidth results in these compounds (see Sec. III). The solution of this problem probably lies in the assumed energy independence of the matrix elements, which are simply represented by the term V in Eq. (9), and the inadequacy of the Debye approximation. In any case, assuming $\Delta H_{pp}\sim 1/T_1$ and choosing

$$\frac{3}{\gamma\pi^3\rho^2 v^{10}}\frac{V^4}{\hbar^5}\frac{k^5}{\hbar^5}=1.8\times10^{-12}$$

in units of G K^{-5} (as compared to the value 1.19×10^{-10} G K^{-5} of Ref. 31 for Mn:SrF_2 at low temperatures) we get a surprisingly good fit between our estimated ΔH_{pp} and $T^5 I_4(T/\Theta_D)$ dependence between 300 and 800 K (Fig. 19). The deviation above 800 K might well result from the increasing anharmonicity to the lattice vibrations in the superionic regime.

We must emphasize that the two-phonon, spin-lattice relaxation rates observed in Mn:$SrCl_2$ are at least 2 orders of magnitude larger than the upper limit on the line broadening in Mn:$KMgF_3$ at high temperatures. Hence we are led to believe that the magnitude of the $T^5 I_4(T/\Theta_D)$ coefficient in Mn:$SrCl_2$ must represent an *enhanced* Raman scattering associated with the softness of the fluorite lattices combined with the effects of covalency.

2. *Concentration-dependent broadening—Mn:XF_2*

Since the corrected integrated intensities do not vary with T in the Mn:XF_2 compounds, unlike the Mn:$SrCl_2$ case, one can immediately conclude that quasistatic crystal-field broadening is unimportant in these systems. Indeed, when the ^{19}F transferred hfs collapses, the linewidth in all of the XF_2 compounds seems to be dominated by concentration-dependent effects, although a smaller, residual c-independent broadening is present at higher temperatures. Here we concentrate on the c-dependent part of ΔH_{pp} and, in particular its behavior in Mn:PbF_2.

(a) Temperature-independent (dipolar) broadening. In the region of temperature above which the ^{19}F transferred hfs collapses, the temperature-*independent* part of the c-dependent broadening was determined as shown in Sec. III C 2. The *upper* bounds established for the Mn^{2+}-Mn^{2+} dipolar broadening may then be compared with the standard ("naive") second (M_2) and fourth (M_4) moment calculations for the linewidth using an assumed truncated Lorentzian line profile, as is appropriate in the dilute limit.[32,33] It was found that the predicted linewidths exceeded the observed ones by approximately a factor of 2 unless (a) Mn^{2+} spins with different values of $m^{(55)}$ were considered unlike and (b) exchange-coupled nearest neighbors were omitted from the calculations of M_2 and M_4. The details of these calculations are given elsewhere.[34] Table II collects the experimental, naive, and corrected values of the dipolar-induced, rigid-lattice linewidths.

(b) Temperature-dependent (collision) broadening. As explained in Sec. III C, the EPR of Mn:PbF_2, in particular, exhibits a contribution to ΔH_{pp} which is *both* c and T dependent. For *fixed* Mn^{2+} ions, any two-body interaction would be linear in c, at small c, but should be T independent. In liquids, spin-exchange collisions between paramagnetic ions are manifest through a collapse of the ^{55}Mn hfs (Refs. 35 and 36) and results in rather unusual c and T dependences to the hfs and linewidth. (We return to the relation of our results to those in the liquids in Sec. V.) To our knowledge, no combined c- and T-dependent EPR linewidth in a *solid* has previously been reported.

The behavior of the Mn^{2+} EPR linewidth in PbF_2, as to its c and T dependence is, in many ways, quite similar to the ^{19}F NMR results on $(1/T_1)$ and $(1/T_2)$ in this same system.[5,6] There it was shown that $(1/T_1)$ and $(1/T_2)$ vary linearly with the Mn^{2+} concentration and exhibit striking temperature dependences. Their behavior has been ascribed to a collision (or impact) mechanism in which the spin-dephasing—induced relaxation results from nearest-neighbor encounters between "fixed" Mn^{2+} ions and the diffusing F^- ions via the ^{19}F transferred-hfs interaction $\vec{I}\cdot\overleftrightarrow{A}\cdot\vec{S}$. An elaborate model theory was constructed to explain the magnitude and temperature dependence of the ^{19}F NMR relaxation which depends upon $\overleftrightarrow{A}$, the lattice topology, the F^- hopping rate w^-, the Mn^{2+} electronic T_1 (and/or T_2), and both the nuclear and electronic Zeeman energies. With it, a quite favorable comparison was found between theory and experiment.[6]

TABLE II. Experimental (1), "naively" calculated (see text) (2), and corrected (3) values of the rigid-lattice dipolar broadening of Mn^{2+} in the various fluorites per mol % of Mn^{2+} doping. In the corrected calculations (3), Mn^{2+} ions with different values of $m^{(55)}$ are considered "unlike" and the contributions of nearest neighbors to the second and fourth moments are deliberately excluded. See Ref. 34.

	ΔH_{pp}^{dip} (G/at. % dopant)		
	(1)	(2)	(3)
CaF_2	$\lesssim 30$	52	29
SrF_2	$\lesssim 32$	43.5	24.2
PbF_2	$\lesssim 22$	40.5	22
$SrCl_2$	$\lesssim 15$	25	13.9

Clearly, F^- diffusion *cannot* be responsible for the c- and T-dependent EPR linewidth. We are led to assume that Mn^{2+} diffusion, albeit much slower than that of the F^-, must make possible spin-dephasing encounters via the Mn^{2+}-Mn^{2+} dipolar interaction. Without independent information as to the mechanism for impurity cation diffusion and its rate w_I^+ as a function of T, it would be premature to attempt as sophisticated a treatment of the collision broadening in the EPR case as was done for the ^{19}F NMR—particularly so because of the limited region of temperature in which this mechanism dominates all other linewidth contributions. Instead, we give a simple description of the impact broadening which disregards the details of the diffusion process and the precise nature of the "encounter" between the two Mn^{2+} spins.

Suppose that, as a Mn^{2+} diffuses through the lattice, it arrives at some critical distance R_c of another Mn^{2+}. If R_c is small enough such that the magnitude of the dipolar field $H_d(R_c)$ satisfies the inequality

$$\gamma H_d(R_c)\tau > \pi \ , \tag{12}$$

then the precessional phase of both spins will be drastically altered as they are suddenly subject to the resultant field $\vec{H}_r(R_c)=\vec{H}_0+\vec{H}_d(R_c)$. Here τ is the residence time of the Mn^{2+} ion ($\tau^{-1}\equiv w_I^+$). Hence the transverse relaxation time T_2 associated with the spin-dephasing collisions in this slow-hopping limit will simply be the average lifetime between encounters.[5,6] We have

$$T_2=(Z_e c w_I^+)^{-1} \ . \tag{13}$$

By Z_e we designate some effective number of cation sites within a sphere of radius R_c, centered on a given Mn^{2+}, such that Eq. (12) is satisfied. Equation (13) predicts that the linewidth $\Delta H\equiv(\gamma T_2)^{-1}$ will increase linearly with increasing c and w_I^+. In this slow-hopping limit, the collision-induced broadening is independent of the coupling constant $H_d(R_c)$. Since the data contained in Figs. 6 and 10 show the linewidth to be increasing with increasing T (and hence w_I^+) the slow limit must extend to at least 800 K. Figure 11 allows $[d(\Delta H)/dc]$ vs T to be determined; the results are collected in Table III. It remains to estimate Z_e. We arbitrarily assume the spin dephasing to occur only when the Mn^{2+} are either nearest or next-nearest neighbors (NNN) to each other; hence $Z_e=18$. Using the relation $w_I^+(T)=\gamma\Delta H/Z_e c$ and the values of $\Delta H/dc$ given in Table III, one can calculate $w_I^+(T)$ (see Table III). One can test the consistency of the assumption of $Z_e=18$ in the following way. The magnitude of the dipolar field at NNN position $H_d(R_{\rm NNN})=220$ G. When the hopping rate w_I^+ is equal to $\gamma H_d(R_{\rm NNN})\simeq 3.9\times 10^9$ sec^{-1} the linewidth would have its maximum value, for a given value of c. Taking $Z_e=18$, $c=0.01$, we estimate $(\Delta H)^c_{\rm max}\lesssim 30$ G which is to be compared with observed collision-induced broadening $(\Delta H)^c_{\rm max}\simeq 26$ G. This agreement is surely fortuitious in view of the simplicity of our treatment but it does establish the reasonableness of the assumptions that have been made.

TABLE III. Concentration dependence $d(\Delta H)/dc$ of EPR linewidths of Mn^{2+} and its estimated hopping rates w^+ in PbF_2 at various temperatures. For sake of comparison, the fluorine hopping rate w^- is also given.

T (K)	$d(\Delta H)/dc$ (G at.% dopant) ±20%	w^+ (10^9 sec^{-1}) ±30%	w^- (10^9 sec^{-1})
650	10.5	1.0	7.0
675	18.3	1.8	15.0
700	21.0	2.1	25.0
750	25.0	2.5	60.0
800	26.0	2.6	85.0

At the temperature corresponding to the maximum in ΔH, $T\simeq 825$ K, we can compare the F^- and Mn^{2+} hopping rates $w^-/w_I^+\simeq 25$. Although it is comforting to find $w^- \gg w_I^+$, it certainly makes suspect a picture of a static cation sublattice, at least as regards the Mn^{2+} impurities. Setting aside all other differences (size, binding, etc.) between Pb^{2+} and Mn^{2+} ions, one would expect the more massive Pb^{2+} ion to diffuse more slowly so that, quite possibly $w^-/w_{Pb^{2+}} > 100$ at 825 K.

V. SUMMARY AND DISCUSSION

Our high-temperature studies have revealed some interesting properties associated with the EPR of Mn^{2+} in fluorite-type ionic crystals; the most striking of which are the collapse of the ligand transferred hfs and the temperature and/or Mn^{2+} concentration dependence to the linewidth. For completeness, a summary of all processes that contribute to the broadening of the individual Mn^{55} hfs components in the EPR of Mn^{2+} in the XF_2 and $SrCl_2$ compounds is given in Table IV. One might wonder as to whether the newly observed behavior is peculiar to materials which exhibit superionic conductivity. The evidence obtained so far would suggest that indeed this is the case, since earlier studies on MgO (Ref. 35) and $KMgF_3$ (Refs. 7 and 35), for example, gave no evidence of any increase in linewidth or transferred-hfs collapse at high temperatures. Hence significant anion hopping (disorder) and enhanced lattice anharmonicity appear to be prerequisites for the behavior referred to above,

TABLE IV. A summary of all of the line-broadening mechanisms that have been identified in the Mn:XF_2 and Mn:$SrCl_2$ EPR studies.

Line-broadening mechanisms	Magnitude (G/at. % dopant)	c dependence	T dependence	Systems in which expected or identified
^{19}F-Mn^{2+}; dipolar	2–3	None	None	All XF_2
Mn^{2+}-Mn^{2+}; dipolar (static)	14–29 (Mn)	Linear, for $c < 10^{-2}$	None	All XF_2:$SrCl_2$
Unresolved ^{19}F; $^{35,36}Cl$ transferred hfs	9–12; $\lesssim 3$	None	For T such that $w^- \gtrsim A$[19]	All XF_2
Quasistatic crystal-field distortions	$\gg 100$ for $\pm\frac{1}{2}\leftrightarrow\frac{3}{2}$ or $\pm\frac{3}{2}\leftrightarrow\frac{5}{2}$; 0–30 for $\frac{1}{2}\leftrightarrow-\frac{1}{2}$	None	Strong at moderate T but vanishes when $w^- \gg D$	Only $SrCl_2$—also results in intensity variations with T
Dynamic, anharmonic phonon broadening	0–50	None	Increases with T nonlinearly	$SrCl_2$, PbF_2
Mn^{2+}-Mn^{2+} "collision" broadening	0–40 (Mn)	Linear for $c \lesssim 10^{-2}$	Strong; maximum when $w^+ \simeq \gamma H_d$	PbF_2, CaF_2, and BaF_2

both of which are hallmarks of the superionic conductor. We may well expect results similar to those reported here in other superionic materials (e.g., Mn^{2+} in $PbSnF_4$).

It is instructive to compare the results of our studies with the extensive literature on Mn^{2+} EPR in liquids[10,11,29] and magnetically dilute molten salts.[36,37] Of particular interest is the narrowing of the ^{55}Mn hfs under exchange collisions between pairs of Mn^{2+} ions in the molten salt. First, it must be noted that in the liquid (or molten salt) the rate ω_l, which characterizes the particle motion, and therefore determines both the frequency of exchange collisions and crystal-field modulation, is usually much larger than Zeeman or ^{55}Mn hfs frequencies and is comparable to exchange frequencies (i.e., $\omega_l \gg \omega_0$ or $A^{(55)}/\hbar$ and $\omega_l \approx \omega_{ex}$). In the solid, even at the highest temperatures, the situation is quite the opposite. These two regimes are referred to as the "fast" and "slow" limits, respectively,[10] in dynamic crystal-field narrowing (broadening) of Mn^{2+} EPR lines in liquids.

In regard to ^{55}Mn hfs, what is seen in the molten salts is the exchange narrowing of a single hyperfine broadened line,[36,37] i.e., $\Delta\omega = \langle\omega_{hfs}^2\rangle/\omega_{ex}$, where ω_{ex} is a function of the "hopping" rate, T, the viscosity and the probability that an encounter between two Mn^{2+} spins will result in a phase interruption, as well as the Mn^{2+} concentration. In the "slow" limit, which is appropriate to the superionic solid, and where a completely resolved ^{55}Mn hfs is present, one might expect exchange collisions to produce a broadening and an accompanying slow collapse of the ^{55}Mn hfs. The fact that there is absolutely no evidence for the collapse of the ^{55}Mn hfs in PbF_2, as a function of c and T, leads us to the following conclusion: *The diffusing Mn^{2+} ions never occupy nearest-neighbor cation positions simultaneously so as to make an exchange collision possible.* One possible explanation for this tendency of one Mn^{2+} to avoid another at closest range is that the ionic radius of Mn^{2+} (0.8 Å) is so much smaller than that of Pb^{2+} (1.2 Å). Having two Mn^{2+} as NN would result in such a large, local strain deformation that it would be energetically too costly to do so. Perhaps this argument would also be offered in explanation of the low solubility of Mn^{2+} in PbF_2.

The comparison of the hopping rates for the F^- and Mn^{2+} ions in PbF_2 given in Table III requires further comment. The F^- motion is associated with Frenkel defect formation and is an activated process; its large variation with T in the range 650–800 K is a direct consequence of this fact. The fact that the Mn^{2+} hopping rate appears to vary so little in the same range of T suggests that it is *not* an activated process but results indirectly from the large anion disorder in the superionic region. Thus we expect that below 600 K Mn^{2+} diffusion would decrease precipitously in PbF_2. It would be useful to have a Mn tracer diffusion study at lower T in Mn:PbF_2.

We note that our conclusion of anharmonic phonon processes rather than dynamic crystal-field modulation being responsible for the (c-independent) T-dependent broadening in $SrCl_2$ as well as PbF_2 differs from those of an earlier study on PbF_2.[7] The latter work did not have the advantage our studies had in working at two frequencies and with dif-

ferent superionic conductors. The linewidth results in Mn:$SrCl_2$ are particularly dramatic and, since they are so much larger in magnitude than any of the fluorides, suggest that covalency plays an important role in the spin-phonon coupling. Finally, we remark on our choice of a model for dynamic–crystal-field modulation which concentrates on the motion of the *vacancy* rather than the particle. The justification for this is that the cubic crystal field is distorted only when a vacancy is present; in the first approximation, it does not matter if two anions exchange position and left the field cubic. This reasoning is peculiar to the crystal-field problem because, in discussing NMR, conductivity, or the collapse of the transferred hfs, the distinction between particle and vacancy need not be made, provided the ratio of the two is kept in mind. Again, in discussing crystal-field modulation in a liquid, no distinction is made, but there it is a consequence of "vacancy" and "particle" concentration being identical as are transit and residence times.

ACKNOWLEDGMENTS

We thank Dr. A. R. King for useful discussions, Dr. R. D. Hogg for technical assistance, and N. Nighman for the preparation of all materials. This research was supported in part by U.S. Department of Energy Contract No. DOE-E34-PA-244.

APPENDIX A: AUTOCORRELATION FUNCTION $\langle D(0)D(t)\rangle$ OF THE AXIAL CRYSTAL FIELD IN A SUPERIONIC CONDUCTOR

For simplicity, we take the following as a model for the axial distortions of the cubic crystal field that occur when a vacancy resides at any near-neighbor anion site to a Mn^{2+}. If the vacancy is present, then the axial field can take on the values $\pm D$ and is zero otherwise. Let $p_1(t)$, $p_2(t)$, and $p_3(t)$ be the respective probabilities that at time t the axial field is $+D$, 0, or $-D$. If w is the anion-hopping rate, then the vacancy-hopping rate is w/c, where c is the vacancy concentration. Neglecting the probability of a transition directly from D to $-D$ or vice versa, the rate equations can be written as follows:

$$\frac{dp_1}{dt}=w\left[-\frac{1}{c}p_1+\frac{1}{2}p_2\right], \tag{A1a}$$

$$\frac{dp_2}{dt}=w\left[\frac{1}{c}p_1-p_2+\frac{1}{c}p_3\right], \tag{A1b}$$

$$\frac{dp_3}{dt}=w\left[\frac{1}{2}p_2-\frac{1}{c}p_3\right]. \tag{A1c}$$

The $\frac{1}{2}$ factor in Eqs. (A1a) and (A1c) results from the equal probability of switching from 0 to D or 0 to $-D$.

These coupled, first-order differential equations are solved by first noting that

$$\frac{dp_2}{dt}=w\left[\frac{1}{c}(1-p_2)-p_2\right]$$

$$=-w\left[1+\frac{1}{c}\right]p_2+\frac{1}{c}w\ .$$

The general solution of this equation is given by

$$p_2(t)=\frac{1}{1+c}+A_2e^{-w(1+1/c)t}, \tag{A2}$$

where A_2 is determined by the initial conditions.

Subtracting Eq. (A1c) from (A1a), we obtain

$$\frac{d}{dt}(p_1-p_3)=-\frac{w}{c}(p_1-p_3)\ ,$$

so that

$$p_1(t)-p_3(t)=A_0e^{-w/ct}, \tag{A3}$$

where again A_0 is determined by specifying the initial conditions. Finally,

$$p_1(t)+p_3(t)=1-p_2(t)$$

$$=\frac{c}{1+c}-A_2e^{-w(1+1/c)t},$$

so that

$$p_{1,3}(t)=\frac{c}{2(1+c)}\frac{1}{2}(A_0\mp A_2e^{-wt})e^{-(w/c)t}. \tag{A4}$$

Generally, the autocorrelation function of the axial field $D(t)$ will be given by [assuming $D(t)$ to be real]

$$\langle D(0)D(t)\rangle=\langle D(0)[Dp_1(t)+Dp_2(t)-Dp_3(t)]\rangle\ . \tag{A5}$$

The probability that $D(0)=\pm D$ is $\frac{1}{2}[c/(1+2)]$ and that $D(0)=0$ is $1/(1+c)$. The case where $D(0)=0$ does not contribute to $\langle D(0)D(t)\rangle$; when $D(0)=D$, we get $p_1(0)=1$, $p_2(0)=p_3(0)=0$, and $A_2=-1/(1+c)$, $A_0=1$. When $D(0)=-D$, A_2 remains the same and $A_0=-1$. Let $p_{a1}(t)$ and $p_{a3}(t)$ be equal to $p_1(t)$ and $p_3(t)$, respectively, when $D(0)=D$ and let $p_{b1}(t)$ and $p_{b3}(t)$ be equal to $p_1(t)$ and $p_3(t)$, respectively, when $D(0)=-D$. Then from Eq. (A5), we have

$$\langle D(0)D(t)\rangle=\frac{1}{2}\frac{c}{1+c}\{D^2[p_{a1}(t)-p_{a3}(t)]$$

$$-D^2[p_{b1}(t)-p_{b3}(t)]\}$$

or

$$\langle D(0)D(t)\rangle = \frac{cD^2}{1+c}\left[1+\frac{e^{-wt}}{1+c}\right]e^{-(w/c)t}. \quad \text{(A6)}$$

Note that the autocorrelation function decays (effectively) at the vacancy-hopping rate w/c and not the anion-hopping rate w, and its apparent amplitude is $\sqrt{c}/(1+c)\,D$ and not D.

[1]R. B. Boyce and B. A. Huberman, Phys. Rep. 51, 189 (1979).

[2]*Physics of Superionic Conductors,* edited by M. B. Salomon (Springer, Berlin, 1979).

[3]*Crystals with the Fluorite Structure,* edited by W. Hayes (Clarendon, Oxford, 1974).

[4]*Fast Ion Transport in Solids,* edited by P. Vashishta, J. N. Mundy, and G. K. Shenoy (Elsevier-North Holland, New York, 1979).

[5]R. D. Hogg, S. P. Vernon, and V. Jaccarino, Phys. Rev. Lett. 39, 481 (1977).

[6]S. P. Vernon, P. Thayamballi, R. D. Hogg, D. Hone, and V. Jaccarino, Phys. Rev. B 24, 3756 (1981).

[7]C. Evora and V. Jaccarino, Phys. Rev. Lett. 39, 1554 (1977). It was established here that the EPR spectrum is consistent with Mn:PbF_2 being in the β (cubic) phase.

[8]R. J. Richardson, S. Lee, and T. J. Menne, Phys. Rev. B 4, 3837 (1971); R. Lacroix, Helv. Phys. Acta 30, 374 (1957).

[9]The degree of cancellation obviously depends on $A^{(55)}$ and H_0 and is not total—at least as can be seen from third-order perturbation theory. Luckhurst and Pedulli (Ref. 11) found the same cancellation when they numerically calculated the fields corresponding to the $|M-1,m\rangle \leftrightarrow |M,m\rangle$ transitions by finding the eigenvalues of the appropriate 36×36 matrix, without resorting to perturbation theory. They do not indicate whether or not the cancellation is total or accidental.

[10]G. R. Luckhurst, in *Electron Spin Relaxation in Liquids,* edited by T. L. Muus and P. W. Atkins (Plenum, New York, 1972).

[11]G. R. Luckhurst and G. F. Pedulli, Mol. Phys. 22, 931 (1968).

[12]R. J. Richardson, S. Lee, and T. J. Menne, Phys. Rev. B 6, 1065 (1972).

[13]P. W. Anderson, J. Phys. Soc. Jpn. 9, 316 (1954); P. W. Anderson and P. R. Weiss, Rev. Mod. Phys. 25, 269 (1953).

[14]C. P. Slichter, *Principles of Magnetic Resonance,* 2nd ed. (Springer, Berlin, 1978), Appendix F and references therein.

[15]M. Beniere, M. Chemla, and F. Beniere, J. Phys. Chem. Solids 40, 729 (1979).

[16]G. M. Hood and J. A. Morrison, J. Appl. Phys. 38, 4796 (1967).

[17]E. Dormann, D. Hone, and V. Jaccarino, Phys. Rev. B 14, 2715 (1976).

[18]C. Evora, Rev. Sci. Instrum. 51, 663 (1980).

[19]C. P. Slichter, *Principles of Magnetic Resonance,* Ref. 14.

[20]M. Peter, D. Shaltiel, J. H. Wernick, H. J. Williams, J. B. Mock, and R. C. Sherwood, Phys. Rev. 126, 1395 (1962).

[21]S. P. Vernon and V. Jaccarino (unpublished).

[22]D. R. Figueroa, A. V. Chadwick, and J. H. Strange, J. Phys. C 11, 55 (1978).

[23]J. Boyce, J. C. Mikkelsen, and M. O'Keeffe, Solid State Commun. 21, 955 (1977).

[24]W. Low, *Paramagnetic Resonance in Solids* (Academic, New York, 1960), pp. 39—57.

[25]V. Beltran-Lopez and J. Castro-Tello, J. Magn. Res. 39, 437 (1980).

[26]C. P. Slichter, *Principles of Magnetic Resonance,* Ref. 14, Secs. 5.6 and 5.7.

[27]A. G. Redfield, in *Advances in Magnetic Resonance,* edited by J. S. Waugh (Academic, New York, 1965), Vol. 1.

[28]M. H. Dickens, W. Hayes, C. Smith, and M. T. Hutchings, in *Fast Ion Transport in Solids,* edited by P. Vashishta, J. Mundy, and G. K. Shenoy (Elsevier-North Holland, New York, 1979), p. 225.

[29]G. Luckhurst and G. F. Pedulli, Chem. Phys. Lett. 7, 49 (1970).

[30]A. Abragam and B. Bleaney, *Electron Paramagnetic Resonance of Transition Metal Ions* (Clarendon, Oxford, 1970), Chap. 10.

[31]J. B. Horak and A. W. Nolle, Phys. Rev. 153, 372 (1967).

[32]J. H. Van-Vleck, Phys. Rev. 74, 1168 (1948).

[33]A. Abragam, *Principles of Nuclear Magnetism,* (Clarendon, Oxford, 1961), Chap. IV, Sec. IV.

[34]J. Shinar and V. Jaccarino, Phys. Lett. 91A, 132 (1982).

[35]W. M. Walsh, J. Jeener, and N. Bloembergen, Phys. Rev. 139, A1338 (1965).

[36]L. Yarmus, M. Kukk, and B. R. Sundheim, J. Chem. Phys. 40, 33 (1964).

[37]T. B. Swenson, J. Chem. Phys. 45, 179 (1966).

[38]M. Blume and R. Orbach, Phys. Rev. 127, 1587 (1961).